Early peak and rapid decline of SARS-CoV-2 seroprevalence in a Swiss metropolitan region

Marc Emmenegger[1], Elena De Cecco[1], David Lamparter[2,#], Raphaël P. B. Jacquat[3,4,#], Daniel Ebner[5], Mathias M. Schneider[3], Itzel Condado Morales[1], Dezirae Schneider[1], Berre Doğançay[1], Jingjing Guo[1], Anne Wiedmer[1], Julie Domange[1], Marigona Imeri[1], Rita Moos[1], Chryssa Zografou[1], Chiara Trevisan[1], Andres Gonzalez-Guerra[1], Alessandra Carrella[1], Irina L. Dubach[6], Christian L. Althaus[7], Catherine K. Xu[3], Georg Meisl[3], Vasilis Kosmoliaptsis[8,9], Tomas Malinauskas[10], Nicola Burgess-Brown[11], Ray Owens[10,12], Stephanie Hatch[5], Juthathip Mongkolsapaya[13], Gavin R. Screaton[13], Katharina Schubert[14], John D. Huck[15], Feimei Liu[15], Florence Pojer[16], Kelvin Lau[16], David Hacker[16], Elsbeth Probst-Müller[17], Carlo Cervia[17], Jakob Nilsson[17], Onur Boyman[17,18], Lanja Saleh[19], Katharina Spanaus[19], Arnold von Eckardstein[19], Dominik J. Schaer[6], Nenad Ban[14], Ching-Ju Tsai[20], Jacopo Marino[20], Gebhard F. X. Schertler[20,21], Nadine Ebert[22,23], Volker Thiel[22,23], Jochen Gottschalk[24], Beat M. Frey[24], Regina Reimann[1], Simone Hornemann[1], Aaron M. Ring[15], Tuomas P. J. Knowles[3,4], Ioannis Xenarios[2,25], David I. Stuart[10], and Adriano Aguzzi[1*]

[1] Institute of Neuropathology, University of Zurich, 8091 Zurich, Switzerland

[2] Health2030 Genome Center. 9 Chemin des Mines, 1202 Geneva, Switzerland

[3] Centre for Misfolding Diseases, Department of Chemistry, University of Cambridge, Lensfield Road, Cambridge CB2 1EW, United Kingdom

[4] Cavendish Laboratory, Department of Physics, University of Cambridge, JJ Thomson Ave, Cambridge CB3 0HE, United Kingdom

[5] Target Discovery Institute, University of Oxford, OX3 7FZ, England

[6] Division of Internal Medicine, University Hospital Zurich, 8091 Zurich, Switzerland

[7] Institute of Social and Preventive Medicine, University of Bern, 3012 Bern, Switzerland

[8] Department of Surgery, Addenbrooke's Hospital, University of Cambridge, Hills Road, Cambridge CB2 0QQ, United Kingdom

[9] NIHR Blood and Transplant Research Unit in Organ Donation and Transplantation, University of Cambridge, Hills Road, Cambridge CB2 0QQ, United Kingdom

[10] Division of Structural Biology, The Wellcome Centre for Human Genetics, University of Oxford, Headington, Oxford, OX3 7BN, UK

[11] Structural Genomics Consortium, University of Oxford, Oxford, OX3 7DQ, UK

[12] The Rosalind Franklin Institute, Harwell Campus, OX11 0FA, UK

[13] Nuffield Department of Medicine, Wellcome Trust Centre for Human Genetics, University of Oxford, Oxford, UK

[14] Department of Biology, Institute of Molecular Biology and Biophysics, ETH Zurich, Zurich, Switzerland

[15] Department of Immunobiology, Yale School of Medicine, New Haven, CT, USA

[16] Protein Production and Structure Core Facility, EPFL SV PTECH PTPSP, 1015 Lausanne, Switzerland

[17] Department of Immunology, University Hospital Zurich, 8091 Zurich, Switzerland

[18] Faculty of Medicine, University of Zurich, 8006 Zurich

[19] Institute of Clinical Chemistry, University Hospital Zurich, 8091 Zurich, Switzerland

[20] Department of Biology and Chemistry, Laboratory of Biomolecular Research, Paul Scherrer Institute, 5303 Villigen-PSI, Switzerland

[21] Department of Biology, ETH Zürich, 8093 Zürich, Switzerland

[22] Institute of Virology and Immunology, 3012 Bern, Switzerland

[23] Department of Infectious Diseases and Pathobiology, Vetsuisse Faculty, University of Bern, 3012 Bern, Switzerland

[24] Regional Blood Transfusion Service Zurich, Swiss Red Cross, 8952 Schlieren, Switzerland

[25] Agora Center, University of Lausanne, 25 Avenue du Bugnon, 1005 Lausanne

[#] equal contribution

*to whom correspondence should be addressed: adriano.aguzzi@usz.ch

Abstract

Serological assays can detect anti-SARS-CoV-2 antibodies, but their sensitivity often comes at the expense of specificity. Here we developed a Tripartite Automated Blood Immunoassay (TRABI) to assess the IgG response against SARS-CoV-2. Calibration was performed with 90 prepandemic and 55 virologically and clinically confirmed COVID-19 samples. Posterior probabilities were calculated from 3x8 measurements of logarithmically diluted samples against the ectodomain and the receptor-binding domain of the spike protein and the nucleocapsid protein. We then performed 948'528 assays on 5'503 prepandemic and 34'019 copandemic samples from hospital patients and healthy blood donors. The seroprevalence increased in March 2020 (0.3%; $CI_{95\%}$: 0.1% - 0.5%) among hospital patients but plateaued in April at 1.1-1.3%, and dropped to 0.3-0.7% in July. A dynamic transmission model describing SARS-CoV-2 transmission and seroconversion in the general population of the Canton of Zurich yielded an infection fatality ratio of 0.6% ($CI_{95\%}$: 0.4%-0.8%), similarly to other European areas. While the evolution of seroprevalence points to a high effectiveness of containment measures, our data highlight that antibody waning warrants a continuous seromonitoring to reliably estimate the prevalence in a population.

Introduction

Within just a few months of the onset of severe acute respiratory syndrome coronavirus 2 (SARS-CoV-2) pandemic, several million cases and hundreds of thousands of fatalities from coronavirus disease 2019 (COVID-19) have been registered. It has also indirectly caused many more deaths by hijacking healthcare resources, thereby making them unavailable to patients suffering from other diseases. In addition, COVID-19 has created profound economic distress for most travel-related industries. Finally, it has disrupted a plethora of industrial supply chains, resulting in a massive worldwide unemployment crisis that will cost many more human lives.

In order to alleviate the direct consequences of the SARS-CoV-2 pandemic, governments and public healthcare agencies need granular and reliable data on the prevalence of infection, the incidence of new infections, and the spatial-temporal oscillations of these parameters within regions of interest. The acquisition of such data, however, is daunting and data are prone to misinterpretation (1). Firstly, data needs to be acquired extremely rapidly. Secondly, their usefulness is dependent on being representative of large populations, meaning that they need to be acquired in massive numbers. Finally, the tolerance of false-positives and false-negatives must be extremely low in order to ensure an accurate estimation of the prevalence; the estimation is particularly challenging in low-prevalence areas.

Intuitively, PCR-based diagnostics would seem suitable to fulfill the above criteria. However, practical experience has shown that this is not the case. The acquisition of representative diagnostic material for PCR has proven challenging, with deep nasal swabs being difficult to perform, uncomfortable for patients and potentially hazardous for medical personnel. Accordingly, the sensitivity of PCR diagnostics is often disappointing, with reported false-negative rates of 25% even under the best conditions (2).

Serological assays, on the other hand, address the adaptive immune responses of the host which are fundamental to limiting viral spread within individuals and populations. While they lag behind the viral infection, they can serve as both powerful epidemiological tools as well as useful clinical aids. Firstly, antibodies can be easily retrieved from many biological fluids, notably including venous and capillary blood. Secondly, antibodies typically persist for several months whereas the viral load in the upper respiratory tract frequently wanes within weeks (3). Importantly, immunological assays can be largely automated, and are thus suitable to mass screening of extremely large cohorts.

Representative testing of entire populations mandates fully automatable assays capable of outputting reliable results at extremely high rates and very low cost. Here we describe an assay that fulfills these criteria. We have screened 39'522 samples for antibodies against three SARS-CoV-2-related antigens: the ectodomain of the spike protein (S), its receptor-binding domain (RBD) and the nucleocapsid protein (NC), using SARS-CoV-2 enzyme-linked immunoassays (ELISA) (4-6). Samples included patients entering the University Hospital of Zurich (USZ), Switzerland, from December 2019 to the present (defined as “copandemic”; n=24’830), a cohort of patients treated at USZ between 2016 and 2018 (“prepandemic”; n=4’407), as well as 1’096 prepandemic and 9’102 copandemic samples from blood donors in Zurich. Our test cohorts were completed by virologically and/or clinically confirmed cases with SARS-CoV-2 infections (31 annotated USZ samples and 56 additionally recruited samples for blood donation service). Our results paint a detailed picture of the spread of the pandemic within the greater Zurich area from February to July 2020, and may be representative of other metropolitan areas that have been weakly affected by SARS-CoV-2 despite a highly mobile population served by large international airports.

Results

TRABI: a miniaturized high-throughput ELISA for multiple SARS-CoV-2 antigens.

The goal of this project was to assess the rate of seroconversion throughout the course of the pandemic in tens of thousands of individuals who may have been exposed to SARS-CoV-2. This requires high specificity of the assay procedure in order to avoid false-positive results, while not compromising its sensitivity and risking to underestimate the prevalence of anti-SARS-CoV-2 antibodies. Equally crucial is the ability to maintain a throughput of >4'000 samples/24h, and to minimize the costs of reagents and labor. We achieved these goals (1) by testing for multiple viral antigens, (2) by employing extensive automation including contactless fluid-handling, (3) by reducing the sample volumes to the nanoliter scale, and (4) by combining multiple antigen measurements via statistical techniques. The TRABI assay described below utilizes contactless acoustic dispensing (7, 8) to transfer droplets (2.5 nl each) of plasma into high-density 1536-well plates (total volume: 3 µl) and measures the IgG response against viral proteins in an immunosorbent format (**Fig. 1A** and **Fig. S1A** for detailed procedure).

In order to identify the most suitable viral targets for TRABI, we infected Vero cells with wild-type SARS-CoV-2 virus. Cell lysates were then subjected to Western blotting using the plasma of patients with confirmed COVID-19 (n=7). The bands corresponding to the S and NC proteins were prominently visible in infected cells, but were undetectable in non-infected cells and were suppressed by adding soluble S and NC antigen to the patient plasma before incubation with the Western blot (**Fig. 1B**). Accordingly, we selected the SARS-CoV-2 spike protein (9), the receptor binding domain (RBD, amino acids 330-532 of the S protein), and the nucleocapsid protein (NC, amino acids 1-419) as target antigens for TRABI. Each sample was tested at eight consecutive two-fold dilution points (1:50 to 1:6400), and the resulting data were fitted to a sigmoidal curve by logistic regression. The inflection point (or $-\log_{10}(EC_{50})$) of each sigmoid was defined as the respective antibody titer.

As reference samples for assay establishment, we utilized a collective of 55 venous plasma samples drawn at various days post onset of symptoms (dpo) from 27 RT-qPCR confirmed patients suffering from COVID-19 and hospitalized at the University Hospital of Zurich (USZ, true positives), as well as 90 anonymized USZ samples from the prepandemic era (true negatives) (see **Table S1**). We then constructed receiver-operating-characteristics (ROC) curves to assess the assay quality for each antigen individually. Finally, we created a composite metric that integrates S/RBD/NC measurements using quadratic discriminant analysis (QDA). While each single antigen showed excellent discrimination of negatives and positives on samples drawn at ≥14 dpo, the

compound models outperformed the individual antigen measurements at 7-13 dpo, where the emergence of an IgG response is expected to be variable (**Fig. 1C**, upper panel). We therefore used the QDA modeling assumptions to infer the prevalence in large cohorts based on the distributional information of true negatives and true positives (details in Methods) using information gained from all three antigens.

To benchmark TRABI, we compared the results with a high-throughput assay under development at the University of Oxford as well as assays commercialized by Roche (Elecsys), DiaSorin, EuroImmun, and Abbott (**Fig. 1C**, lower panel). This comparative assessment was based on 136 of 146 samples (10 samples were removed from the analysis because of insufficient sample volume to perform all tests). While all assays displayed 100% specificity/sensitivity at late time points, TRABI scored best at early time points, also when additionally compared to a lateral-flow assay (**Fig. S2A**). When these results were plotted as a function of dpo, a temporal pattern emerged consistent with the gradual emergence of IgG antibodies within 14 dpo (**Fig. 1D**).

Temporal evolution of the SARS-CoV-2 epidemic in the greater area of Zurich

Due to supply-chain bottlenecks, but also because of the intrinsically narrow window of infectivity, testing of individuals for the presence of SARS-CoV-2 nucleic acids has been limited to those at elevated risk before and after the peak of the epidemic. During that time, individuals with mild symptoms were asked to isolate at home, often without being tested for the presence of SARS-CoV-2 RNA. Thus, the true number of people who underwent an infection with SARS-CoV-2 may at best be a rough estimate modelled on data of numbers of hospitalizations and deaths (10). We are therefore using TRABI to screen a large sample of Swiss urban populations. To date, we have screened 39'522 samples from a University Hospital cohort of Zurich (USZ patient cohort) with diverse diseases (**Table S1**) and from the blood donation service (BDS, see **Table S1**) of Zurich (healthy group), starting from December 2019 (**Fig. S3A, B**).

To reliably measure the prevalence of seroconversion, we used known positives and negatives as internal calibrators for each cohort. These condition-positives/negatives were screened simultaneously to all other samples using exactly the same procedures. Their annotation as condition positives/negatives was performed post-hoc using USZ and BDS databases in the absence of serological data. First, we identified all USZ samples with known positive SARS-CoV-2 RT-qPCR results (n=175). Condition-positive samples (n=31) were defined as those with (1) clinically manifest COVID-19 pneumonia and (2) positive RT-qPCR for SARS-CoV-2 and (3) venipuncture occurring ≥ 14 days after the positive qPCR. To avail of condition-positives from the cohort of blood

donors, 56 samples from convalescent individuals with PCR-confirmed SARS-CoV-2 infection recruited for a plasmapheresis study were included.

To determine potentially unspecific results, e.g. due to cross-reactivity with other coronaviruses, we screened 5'503 prepandemic samples (condition-negatives). For the BDS cohort, we enriched the condition-negatives with 2'100 samples from December 2019 and January 2020 to increase the numbers of the assumed negatives and to obtain a more reliable baseline. We tested two models: the first model assumes that both the condition-positive and negative data follow distinct multivariate Gaussian distribution with unequal covariances (QDA) (**Fig. 2A, B**), whereas the second model is based on Gaussian distributions with equal covariances (LDA) (**Fig. S3C, D**). LDA was additionally performed because it allows to verify the distributional assumptions more readily (**Fig. S3E, F**). Using the distributions of the condition negatives and the condition positives, we computed the posterior probability (i.e. the probability of an individual to be seropositive as modeled via the distribution of the known condition-negatives and known condition-positives) for all data points (see **Fig. S3A, B**). The respective ROC curves were then plotted (**Fig. S3H, I**). At 100% specificity, we identified 27/31 of the annotated true positives for the USZ (**Fig. S3G**) and 37/56 annotated true positives for the BDS cohort (**Fig. S3H**). For the BDS cohort, the sensitivity increased rapidly with a slight decrease in specificity (at a false-positive-rate of 0.001, we identified 52/56 condition positives). We then applied this model to estimate the prevalence in the population. No substantial shift above baseline was inferred for samples screened from January and February (**Fig. 2C** and **Fig. S3I**, USZ cohort). A sudden increase in prevalence manifests in March (QDA: 0.3% (95% confidence intervals: 0.1%-0.5%) and LDA: 0.3% ($CI_{95\%}$: 0.1%-0.5%)) and peaks in April 2020 (QDA: 1.4% ($CI_{95\%}$: 1.0%-1.7%) and LDA: 1.3% ($CI_{95\%}$: 1.0%-1.7%)), in accordance with the virologically and clinically reported rise in SARS-CoV-2 infections in these months. After that, the estimated prevalence started to decline (average value May to beginning of July 0.9% and 0.8% of QDA and LDA, respectively) with variations on a low level. The BDS collective showed a comparable but slightly delayed time course of seroconversion, with the prevalence approximating 1.2% in April (QDA: 1.2% ($CI_{95\%}$: 0.7%-1.8%) and LDA: 1.1% ($CI_{95\%}$: 0.6%-1.7%) and 1.6% in May (QDA: 1.6% ($CI_{95\%}$: 1.0%-2.3%) and LDA: 1.6% ($CI_{95\%}$: 1.0%-2.2%)) (**Fig. 2C** and **Fig. S3I**). After a minimal decrease in June, it drops to 0.7% in early July (($CI_{95\%}$: 0.3%-1.2%) and LDA: 0.7% ($CI_{95\%}$: 0.27%-1.2%)).

In order to address the epidemiological implications of these findings, we employed a dynamic transmission model that describes infection, hospitalization, recovery, death and seroconversion

due to SARS-CoV-2 in the Canton of Zurich (1.5 million). Assuming the BDS samples are representative of the general population in the Canton of Zurich, the model accurately describes the rapid rise in seroprevalence during the second half of March and the month of April (**Fig. 2D** and **Fig. S4**). Using a maximum likelihood framework, we estimated a seroprevalence of 1.6% (95% prediction interval, $PI_{95\%}$: 1.0%-2.2%) by the end of May, and an infection fatality ratio (IFR) of 0.6% ($CI_{95\%}$: 0.4%-0.8%) for the general population in the Canton of Zurich.

To challenge the technical reproducibility of TRABI, we selected 210 high-score samples and 122 random samples from known seronegatives and repeated the assays. The screens proved to be highly replicable when comparing the duplicates from the same screen (S: $R^2 = 0.85$ among samples where both could be adequately fitted, see **Fig. 2E**) and the values from the follow-up screen with the values initially derived from serology (for example, 87% among re-screened samples with a $-\log EC_{50}$ for S above 2.5 had a $-\log EC_{50}$ value above 2 in the second screen, see **Fig. S5**).

Antibodies against the RBD of SARS-CoV can bind to the SARS-CoV-2 RBD (11). We therefore tested whether samples with high anti-SARS-CoV-2-RBD titers display cross-reactivity with SARS-CoV RBD. For visualization, we binned samples into groups of absent, moderate and high SARS-CoV-2 RBD titers ($-\log[EC_{50}]$ <1.5, 1.5-2, and > 2.5, respectively) and computed their respective QDA-derived posterior probability. For individuals with SARS-CoV-2 RBD titers < 2, a small fraction showed binding to SARS-CoV RBD at $-\log(EC_{50}) > 2$ (**Fig. 2F**). However, those with strong binding properties to SARS-CoV-2 RBD (> 2.5) clustered at high values for SARS-CoV RBD, indicating that some anti-SARS-CoV-2 RBD antibodies were cross-reactive to SARS-CoV RBD.

In summary, TRABI identified first cases of SARS-CoV-2 seroconversion in April 2020, consistent with first infections reported in the Zurich area towards the end of February 2020. While data obtained from healthy individuals suggest that around 1.5% of blood donors have been infected despite the absence of anamnestic COVID-19, the serological prevalence was about 5-fold higher than that of RT-qPCR confirmed cases for the same time point. We conclude that at the time of writing, seroconversion within the greater area of Zurich is still exceedingly rare and very far from herd immunity.

Clinical and demographic characteristics of serologically confirmed SARS-CoV-2 infected hospital patients and healthy donors.

Approximately 22% of the USZ samples stem from repeat venipunctures of patients. For the purpose of the following analyses, these samples were not considered (if multiple draws were avail-

able, the one with the highest posterior probability was used). Seropositivity was defined as having a posterior probability > 0.5. USZ cohort had a median age of 55 years (40 – 68) lower and upper quartile respectively) with a median for seropositives of 56 years (42 - 65) (**Fig. 3A** and **Table S1**). BDS cohort for April to July had a median age of 43 years (29 - 54), and seropositives had a median age of 32 (26 - 46) (**Fig. 3B** and **Table S1**). The majority (88%) of patients in the USZ cohort stemmed from the Canton of Zurich (including the city of Zurich), with smaller contributions by Cantons Aargau, Schwyz, St. Gallen, and Thurgau (**Fig. 3C**). Inhabitants of the city of Zurich constituted a comparatively larger proportion of SARS-CoV-2 seropositives than the rest of the Canton of Zurich.

The blood of USZ patients was drawn in 39 clinical departments (**Fig. 3D**), 24 of which treated patients with a posterior probability > 0.5. In absolute counts, most SARS-CoV-2-positive samples were obtained from the Infectious Disease and Hospital Hygiene ward, followed by the departments of Internal Medicine, Medical Oncology and Hematology, and Cardiology. The wide range of medical departments suggests that SARS-CoV-2 seropositive patients do not solely enter the hospital for the treatment of COVID-19 but for any condition that requires the attention of a USZ physician. Seropositivity can be found across all age groups and in both genders (**Fig. 3A**, **B**, **Table S1**) and stays relatively stable for a longer time up (up to 100 days) (**Fig. 3E**), at least in hospital patients with known SARS-CoV-2 positive PCR status. Long-term monitoring of SARS-CoV-2 seropositive individuals will be important to identify comorbidities potentially associated with SARS-CoV-2 infections.

Prevalence of anti-SARS-CoV-2 antibodies in prepandemic samples.

5’503 prepandemic plasma samples (4’407 USZ hospital patients and 1’096 healthy BDS donors) were examined for the presence of cross-reactive antibodies against S, RBD and NC of SARS-CoV-2. Several individuals had a strong antibody response against a single antigen and an absence of binding to other antigens, reflected in a low posterior probability but high -log(EC50) value (**Fig. S3A, B**). We then directly compared prepandemic and copandemic samples in the USZ cohort on the basis of single antigens and their respective posterior probabilities. When focusing on samples with high values for single assays, we observed an enrichment of high posterior probabilities in pandemic but not in the prepandemic group (**Fig. 4A**). Among samples with individual –log(EC_{50}) values above 2 in May and June 2020, 76% (S), 80% (RBD), and 24% (NC) had a posterior probability > 0.5. In the prepandemic samples, maximally 1 sample with an individual assay level above 2 had a posterior probability above 0.5. This enrichment is suggestive of a substantial performance improvement when using the combined metric in the USZ cohort.

We then compared the immunochemical properties of six prepandemic samples with high binding to S, RBD or NC to two samples of confirmed COVID-19 (COVID 1 and 2, see annotation in **Fig. 4A**). The COVID-19 samples, but not the prepandemic samples, recognized in Western blots the S and NC antigens of SARS-CoV-2 expressed by Expi293F (**Fig. 4B** and **Fig. S6A**). Additional ELISAs performed on the same samples confirmed the initial findings (**Fig 4C** and **Fig. S6B**) including intact binding to the RBD. The discrepancy between ELISA and Western Blot suggests that the RBD is a highly conformational epitope lost upon boiling and SDS denaturation.

To further probe the specificity of the findings, we also carried out competitive ELISAs on pre-pandemic and COVID patients. First, we determined plasma concentrations close to the EC_{50}. Then we pre-incubated appropriately diluted samples with various concentrations of S and RBD (0.04-88 and 0.7-1350 nM, respectively). Samples were then transferred onto ELISA plates coated with S, RBD, and NC. The concentration-dependent displacement of the measured optical density was then visualized (**Fig. 4D** and **Fig. S6C**). We found that both soluble S and the RBD caused a concentration-dependent depletion of the RBD in COVID samples. The S signal could not be depleted with RBD, indicating the presence of epitopes other than the RBD. One pre-pandemic sample (#1, see **Fig. S6C**) displayed competition of the S signal with soluble S but not with soluble RBD. Other prepandemic samples did not show competition at all, suggesting that their reactivity was due to high concentrations of low-affinity antibodies cross-reacting with SARS-CoV-2 S.

Identification of seropositives in healthy donors and clonality of anti-S immune response.

TRABI enabled the identification of 57 blood donors that underwent regular blood donation at the blood donation service of Zurich (**Fig. 2B**, **C**) despite clear serological indications of past infection and antibody titers in the same range as those of PCR-confirmed convalescent individuals (**Fig. 5A**). We assessed IgG and IgA antibodies to S, RBD, and NC as well as responses to multiple control antigens, in 4 healthy blood donors and 4 convalescent individuals recruited to the BDS. We observed binding of IgG antibodies in blood donors and convalescent individuals against S, RBD, and NC, with usually lower IgA titers. No binding against the SARS-CoV-2 non-structural-protein 1 (NSP1), or against bovine serum albumin (BSA) was observed.

To further validate the seropositivity in healthy blood donors, we employed an orthogonal methodology which allows antibody/antigen interactions to be probed in solution, without any immobilization of antigens to a surface. Samples of SARS-CoV-2 convalescent individuals, healthy donors and controls were preincubated with fluorescently conjugated RBD protein. We then monitored the increase in the effective molecular weight of an Alexa647-labelled RBD construct in

solution upon complex formation with an antibody present in the patient sample. This was achieved by measuring the associated decrease in its molecular diffusion coefficient upon binding using a microfluidic platform. While no change in diffusion coefficient or the associated hydrodynamic radius was observed in control samples, all ELISA-positive samples from convalescent and healthy donors indicated a clear binding of antibodies to RBD (**Fig. 5B**). We confirmed these findings by using the samples of several healthy blood donors and convalescent individuals as primary antibodies in Western Blot and detected bands for both S and the NC in the Expi293 cells overexpressing the viral proteins but not in the Expi293 control lysate (**Fig. 5C**).

To obtain a rough estimate of the clonality and epitope specificity of the immune response raised against the S protein, we conducted an ELISA-based soluble antigen competition. Competition with the RBD lead to a decrease in ELISA signal for RBD but not for S or NC in both convalescent individuals and healthy blood donors (**Fig. 5D** and **Fig. S7**). Conversely, competition with S decreased the signal for both S and the RBD (**Fig. 5D**), suggesting the presence of antibodies targeting multiple S epitopes, including RBD. Therefore, the immune response against S was polyclonal and involved multiple viral epitopes.

Discussion

The high-throughput pipeline for SARS-CoV-2 serology described above has enabled us to study a cohort of nearly 40'000 samples from the greater area of Zurich over the time span of the pandemic. In view of the critique levelled at past serological studies (1, 12), we have gone to great lengths to assess and validate our technology. For the initial assay calibration, sensitivity was measured using a panel of clinically and RT-qPCR-confirmed SARS-CoV-2 sera (n=55) at various time points after onset of clinical signs and symptoms and 90 negative controls. A blinded comparison with commercial test kits showed that our approach, which combines three individual assays into one single score, was suitable for large-scale epidemiologic studies.

A key question of relevance to public health is the proportion of the population that has already contracted the virus. As a proxy for the estimation of the underlying infection attack rate in the greater area of Zurich, we have used two independent cohorts: (1) unselected patients coming from all clinical departments of USZ and (2) healthy individuals donating blood to local blood banks (BDS). The availability of known positives and negatives in both cohorts allowed us to model the posterior probability from the multiple available antigen measurements, using the respective distributions of these intrinsic controls. Combining the metrics did indeed lead to a power gain, as shown by the enrichment of samples with high posterior probabilities in excess of the single assays during the epidemic. As a possible drawback, the direct modeling of the multivariate distribution of antigen measurements may hinder the detection of deviations from the modeling assumptions. We explored the robustness to modeling assumptions by employing a mixed univariate Gaussian distribution and saw generally good agreement for prevalence estimations. The extent of our sampling bolsters our confidence in the representativity and validity of our results.

In both cohorts, the prevalence of seropositives climbed over the baseline in late March 2020 and peaked at 1.6% in April, with indications for a slight decrease in prevalence. But are our cohorts representative for the population of the greater area of Zurich? On the one hand, the USZ cohort consists mostly of individuals suffering from disparate diseases, some of which may be a consequence of SARS-CoV-2 infections. On the other hand, individuals with acute infections are typically excluded from donating blood. As a consequence, the BDS cohort may be biased against individuals who may have experienced COVID-19 symptoms and refrained from donating. Yet, despite these fundamental differences in their composition, seroprevalence estimates from both cohorts are in good agreement. This observation underscores the presumption that the prevalence reported here is truly representative of the population under study. Clearly, our study would benefit from the inclusion of cohorts with different age architectures, such as e.g. school children

or individuals staying in retirement homes. While such cohorts have not been introduced in this study, the workflow established here could easily be adapted to the investigation of more focal populations.

The low prevalence and the early plateau of SARS-CoV-2 seroconversion in the greater area of Zurich is in stark contrast to harder hit metropolitan areas in Switzerland (Geneva) or Spain (Madrid) that have reached a seroprevalence above 10% (13, 14). The low prevalence between 1% and 2% might be somewhat surprising when considering that Switzerland borders Northern Italy whose prevalence of infection was reported to reach 43% in healthcare workers (15), and no travel restrictions were imposed between the more severely affected areas of Switzerland (Ticino and the Romandie) and Northern Switzerland (16). This illustrates that the implementation of strong non-pharmaceutical interventions (NPIs) around mid-March ('lockdown') successfully prevented further spread of SARS-CoV-2 in Switzerland (10).

When set in relation to the regional numbers of RT-qPCR-positive cases, our cohort-based estimates of the seroprevalence (1.6% ($CI_{95\%}$: 1.0%-2.2% in May 2020 for BDS) are in line with those of more affected regions of Switzerland such as Geneva (seroprevalence: 10.8% ($CI_{95\%}$ 8.2–13.9%) beginning of May 2020 (13)) and are about 5-10 times higher than the respective incidence of overt COVID-19 (10, 16). Likewise, the estimated IFR is in excellent agreement to what was found in the Canton of Geneva, and for Switzerland overall (17, 18). All these estimates reflect a best-case scenario where hospital capacities have never been exceeded and quality of care for critically ill patients could always be ensured.

If the seropositive status is long-lasting, the evolution of anti-SARS-CoV-2 seroprevalence should reflect the cumulative incidence of new infections with a delay of ≤13 DPO. The data presented here are in agreement with hospital surveys suggesting that few transmission events took place in Zurich between April (approx. 2 weeks after the enactment of 'lockdown' measures) and July. The early peak and subsequent decline of seroprevalence in June-July indicates rapid waning of antibodies directed against SARS-CoV-2 antigens. This decline was robust, occurred in both the USZ and BDS cohorts, and is congruent with observations by others (19-21). Assuming that a negligible number of infections occurred in June-July, the population-wide half-life of the TRABI titer is no longer than 2 months, although individual antibody responses may be a function of disease severity (19). If however a significant number of transmissions took place, waning would be considerably more rapid.

This has far-reaching implications for epidemiological assessments. For example, the immunity profile of a population several months after the peak of infections might underestimate the underlying infection attack rate, thereby skewing inferences on the IFR. Consequently, serosurveys repeated over short time windows and extended over multiple months will be necessary to acquire a realistic picture of the immunity status of a population.

A recent publication (22) has shown pre-existing anti-SARS-CoV-2 antibodies in unexposed humans. Our affinity determinations and immunoblots, however, point to fundamental differences between prepandemic seropositivity and the immune responses of SARS-CoV-2-infected individuals. While the latter consistently showed high-affinity responses that were clearly visible in Western blotting, the few seropositive prepandemic sera were unanimously negative in Western blotting, and equilibrium displacement ELISA of one prepandemic plasma sample suggested a much lower affinity despite similar antibody EC_{50} titers. We conclude that any immune response in uninfected individuals, whether it represents cross-reactivity with common-cold coronaviruses or something else, is of inferior quality and may less likely be protective.

It has been proposed that asymptomatic individuals entail a different, weaker immune response to SARS-CoV-2 (23). While follow-up studies including affinity determinations, epitope mapping, and in-depth analyses of the B-cell and T-cell receptor repertoires (described in (24-26)) will paint a more detailed picture, our data suggests that asymptomatic individuals – identified in the collective of healthy blood donors – entail an antibody response comparable to the one seen in individuals with clinical signs of SARS-CoV-2.

Our population-wide screen allows us to address several crucial questions that have been controversially discussed. What is the frequency of truly asymptomatic cases? What is the complete spectrum of clinical signs and symptoms with which SARS-CoV-2-infected individuals present? Many SARS-CoV-2 patients present with monosymptomatic anosmia caused by olfactory neuritis (27), and it is conceivable that other illnesses may represent hitherto unrecognized signs of SARS-CoV-2 infection. Stratifying the results of our screens by clinical parameters (including international classification of diseases (ICD) codes as well as hematological clinical-chemistry values) will become increasingly important in the years to come, e.g. to protect those at risk, to evaluate immune defenses and their possible waning, and to plan vaccination campaigns.

Our study is conceived as a long-term exercise which, given appropriate funding, will be continued for the next several years. In addition to allowing precise monitoring of the population, it will also enable the determination of titer decays in seropositive individuals as a function of demographic indicators and of comorbidities. However, there are societal concerns linked to antibody testing,

and scientists must not downplay them. Serology is a powerful medical and epidemiological instrument, but it can also be misused to stratify the workforce, to discriminate against the non-immune, and even for far more nefarious deeds. Let's study immune responses, but let's not create a dystopian society based on them.

Materials and Methods

Human specimens and data

All experiments and analyses involving samples from human donors were conducted with the approval of the local ethics committee (KEK-ZH-Nr. 2015-0561, BASEC-Nr. 2018-01042, and BASEC-Nr. 2020-01731), in accordance with the provisions of the Declaration of Helsinki and the Good Clinical Practice guidelines of the International Conference on Harmonisation. Specimens were denoted according to the following conventions: *prepandemic samples*: samples collected before December 2019; *COVID samples*: samples from patients with clinically and/or virologically confirmed SARS-CoV-2 infection; *copandemic samples*: any samples collected in December 2019 or thereafter.

Sample acquisition and biobanking

Small volumes (< 100 µL) of heparin plasma samples were obtained from the Institute of Clinical Chemistry at the University Hospital of Zurich as unique bio specimens, biobanked over recent years in a high-throughput liquid biobank. We received a maximum of one sample per patient per month. After one month, another sample from the same individual would be included if the patient visits the hospital and if blood is sent to the Institute of Clinical Chemistry. EDTA plasma from healthy donors was obtained from the Blutspendedienst (blood donation service) Kanton Zürich and Kanton Luzern from donors who signed the consent that their samples can be used for conducting research.

High-throughput serological screening.

In order to test the samples for the presence of IgG antibodies directed against SARS-CoV-2 antigens, high-binding 1536-well plates (Perkin Elmer, SpectraPlate 1536 HB) were coated with 1 µg/mL S or RBD or NC in PBS at 37 °C for 1 h, followed by 3 washes with PBS-T (using Biotek El406) and by blocking with 5% milk in PBS-T (using Biotek MultifloFX peristaltic pumps) for 1.5 h. Three µL plasma, diluted in 57 µL sample buffer (1% milk in PBS-T), were dispensed at various volumes (from 1200 nL down to 2.5 nL) into pre-coated 1536-well plates using contactless dispensing with an ECHO 555 Acoustic Dispenser (Labcyte/Beckman Coulter). Sample buffer was filled up to 3 uL total well volume using a Fritz Gyger AG Certus Flex dispenser. Thereby, dilution curves ranging from plasma dilutions 1:50 to 1:6400 were generated (eight dilution points per patient plasma sample). After the sample incubation for 2 h at RT, the wells were washed five times with wash buffer and the presence of IgGs directed against above-defined SARS-CoV-2 antigens was detected using an HRP-linked anti-human IgG antibody (Peroxidase AffiniPure Goat Anti-Human IgG, Fcγ Fragment Specific, Jackson, 109-035-098, at 1:4000 dilution in sample

buffer). The incubation of the secondary antibody for one hour at RT was followed by three washes with PBS-T, the addition of TMB, an incubation of three minutes at RT, and the addition of 0.5 M H2SO4 (both steps with Biotek MultifloFX syringe technology). The final well volume for each step was 3 µL. The plates were centrifuged after all dispensing steps, except for the addition of TMB. The absorbance at 450 nm was measured in a plate reader (Perkin Elmer, EnVision) and the inflection points of the sigmoidal binding curves were determined using the custom designed fitting algorithm described below.

Counter screening using commercial and custom-designed platforms

We used the following commercial tests for the detection of anti-SARS-CoV-2 antibodies in 55 plasma samples of 27 patients who were diagnosed by RT-PCR to be infected by SARS-CoV-2 as well as 83-90 plasma samples which were collected before December 2019 and, hence, before the start of the COVID-19 pandemics: The double-antigen sandwich electro-chemiluminescence immunoassay from Roche diagnostics (Rotkreuz, Switzerland) was performed with the E801 of the COBAS8000® system (Roche diagnostics, Rotkreuz, Switzerland). The test detects any antibody against the nucleocapsid antigen. The fully automated LIAISON® SARS-CoV-2 chemiluminescence immunoassay from DiaSorin (Saluggia, Italy) detects IgG against the S1/S2 antigens. The SARS-CoV-2 chemiluminescent microparticle immunoassay from Abbott (Abbott Park, IL, USA) detects IgG against the nucleocapsid antigen and was performed on an Architect™ analyser. Two ELISAs from EUROIMMUN (Lübeck, Germany) detect IgA or IgG against the S1 antigen and were performed by the use of a DSX™ Automated ELISA System (DYNEX Technologies (Chantilly, VA, USA). The high-throughput serology assay in Oxford (under development) was carried out in the Target Discovery Institute, University of Oxford. High-binding 384-well plates (Perkin Elmer, SpectraPlate) were coated with 20 µL of 2.5 µg/mL S o/n at 4°C, followed by 3 washes with PBS-T and by blocking with 5% milk in PBS-T for 2 h. Blocking buffer was removed and 20 µL of 1:25 sera diluted in sample buffer (1% milk in PBS-T) was dispensed into S-coated wells then incubated for 2 h at RT. The wells were washed five times with wash buffer and the presence of IgGs directed against S was detected using an HRP-linked anti-human IgG antibody (Peroxidase AffiniPure Goat Anti-Human IgG, Fcγ Fragment Specific, Jackson, 109-035-098) at 1:50,000 dilution in 20 µL sample buffer. The incubation of the secondary antibody for one hour at RT was followed by three washes with PBS-T and the addition of QuantaRed™ Enhanced Chemifluorescent HRP Substrate Kit (Thermo Scientific, Waltham Massachusetts, USA) then in-

cubated for four minutes at RT before the addition of the stop solution. The fluorescence at excitation/emission maxima of ~570/585nm was measured in a fluorescent plate reader (Perkin Elmer, EnVision).

Data analysis.

Data fitting. Data fitting. Eight-dilution points equally spaced on a logarithmic scale are fitted with an equation derived from a simple binding equilibrium. The inflection point (-$\log_{10}EC_{50}$) is extracted from the fit. Baseline and plateau values are fixed by the respective positive and negative controls in a plate-wise fashion and the signal is fitted following these equations:

$$c_{bound} = 1 - \frac{1}{2}\left(c_a c + k_d + 1 - \sqrt{(c_a c + k_d)^2 + 2(k_d - c_a c) + 1}\right) \ ,$$

where c_{bound} , c_a and c are concentration of the antigen-antibody, antigen, and blood concentration respectively.

$$\mathrm{OD}_{\mathrm{signal}} = c_{bound}\,(baseline - plateau) + plateau$$

Data preprocessing. All samples that yielded an $-\log_{10}EC_{50}$ of below –3 on any antigen were labelled as non-fittable and non-detectable. Their dilution curves cannot be differentiated from baseline and therefore only an upper bound for the $-\log_{10}EC_{50}$ can be determined. These samples were therefore excluded from data fitting but were of course included in ROC analysis and prevalence estimation.

QDA, LDA, and Prevalence estimation. Assume that we have data for m samples with known serostatus and antibody measurements, that is, we have $(X_i, Y_i), i = 1, .., m,$ where X_i is the vector of size p (in our case our antigen measurements) and Y_i is a Boolean variable defining group membership (in our case, whether the individual is seropositive or not). The QDA model assumes multivariate normal distributed X_i given Y_i:

$$(X|Y = j) \sim \mathcal{N}_p\left(\mu_j, \Sigma_j\right).$$

Further, the model assumes that the prior, that is, distribution of Y_i , is known s. t. $P[Y = j] = \pi_j$

The quadratic discriminant classifier simply assigns each sample to the group which has the larger posterior $P[Y|X]$, which is proportional to the joint probability $P[Y, X]$.

Therefore, we assign sample i to group 1 if

$$\log(f_{x|y=1}(x_i)) + \log(\pi_1) > \log(f_{x|y=0}(x_i)) + \log(\pi_0),$$

And to group 0 otherwise. To set the prior, one option is to take just the mean of the group sizes. However, this is not an ideal option in our case, where we have an additional n samples with unknown serostatus to classify: The prevalence in the m samples with known serostatus might deviate substantially from the prevalence in population with unknown serostatus. We therefore estimate $\pi_1$directly from the data of unknown serostatus using a simple expectation maximization scheme. Proceeding in an iterative fashion, from a given estimate π_1^k, we define the posterior (E step):

$$t_1^k(x_i) = \frac{\pi_1^k f_{x|y=1}(x_i)}{\pi_1^k f_{x|y=1}(x_i) + (1-\pi_1^k) f_{x|y=0}(x_i)}.$$

Then, we update our estimate of π_1 (M step):

$$\pi_1^{k+1} = \sum_i \frac{t_1^k(x_i)}{n}.$$

After convergence, this yields our estimate of the positive serostatus prevalence in the samples. Note that the sample ordering according to this classifier is independent of the prior and therefore has no impact on an analysis via ROC curves. Further, note that evaluating QDA via ROC analysis, an out of sample scheme should be employed to avoid biased estimates of performance; we chose 10-fold cross-validation throughout. Lastly, note that the strategy does not critically depend on the normality assumption but just requires an estimate for the density functions, $f_{x|y=j}(x_i)$. Even nonparametric estimates could be an option.

For the LDA approach, we first collapse the antigen measurements per samples according to the linear discriminant classifier:

$$z_i = x_i^T \Sigma_0 (\mu_1 - \mu_0),$$

Where Σ_0 is the covariance estimated from the known negatives only and μ_1, μ_0 are the means of the known positives and negatives respectively. The above algorithm is then applied on the

resulting one dimensional variable z_i. 95% confidence intervals were derived by bootstrap drawing 1000 bootstrap samples, where the number of samples drawn from each annotation group (known positives, known negatives and unannotated) was kept constant.

Epidemiological modelling. We adapted a previously described deterministic, population-based model for SARS-CoV-2 transmission in Switzerland (28). Using a maximum likelihood framework, we fitted the model to aggregated daily numbers of hospitalized and ventilated patients, and deaths in the Canton of Zurich from 27 February 2020 to 31 May 2020 (**Fig. S3)**. Data were provided by OpenZH, the specialist unit for open government data from the Canton of Zurich (29). In contrast to the earlier description of the SARS-CoV-2 epidemic in Switzerland overall, we assumed the daily numbers of hospitalized and ventilated patients in the Canton of Zurich to be negative binomially distributed. We also included monthly seroprevalence data from BDS for model inference assuming the positive samples are binomially distributed. We assumed the rate of seroconversion after onset of symptoms to be 1/6 days, i.e., 90% of infected individuals will have detectable antibodies by day 14 after onset of symptoms. All data and code files are available on the following GitHub repository: https://github.com/calthaus/swiss-covid-epidemic.

High-throughput validation screen

For the validation screen, we picked 60 and 150 samples from BDS and USZ, respectively, that had the high average values when summing -logEC_{50} for both Spike and RBD. Additionally, we added 52 and 70 randomly selected prepandemic samples for the BDS and the USZ cohort respectively. We supplemented the three antigens used in the first screen (NC, S, RBD of SARS-SARS-COV-2) with a SARS-CoV RBD antigen. Unlike for the primary screen, we ran all samples in duplicates spread over two independent plates.

Protein production

The proteins were produced and purified at different sites in Zurich (CH), Oxford (UK), Lausanne (CH), and Yale University (USA).

Oxford, SGC. Recombinant proteins were purified as reported previously with small modifications (6, 30). Mammalian expression vectors containing secreted, codon-optimized SARS-CoV-2 S (pHL-Sec (31); aa. 1-1208, C-terminal 8His-Twin-Strep) and RBD (pOPINTTGNeo; aa. 330-532, C-terminal 6His) were transiently transfected with linear PEI into Expi239™ cells cultured in roller bottles in FreeStyle 293 media. Cell culture media was harvested after 3 days at 37°C for RBD or 3 days at 30°C for Spike and then buffered to 1X PBS. Proteins were first pulled down on Ni^{2+} IMAC Sepharose® 6 Fast Flow (GE) with stringent washing (>50 CV with 40 mM imidazole). RBD was polished on a Superdex 75 16/600 column (GE) equilibrated with 1X PBS, while Spike was

directly dialyzed into 1X PBS using SnakeSkin™ 3,500 MWCO dialysis tubing. Proteins were concentrated with VivaSpin® centrifugal concentrators, centrifuged at 21,000 x *g* for 30 min to remove precipitates, and flash frozen at 1 mg/mL

Lausanne, EPFL SV PTECH PTPSP and Zurich UZH. The prefusion ectodomain of the SARS-CoV-2 S protein (the construct was a generous gift from Prof. Jason McLellan, University of Texas, Austin; see (30)) was transiently transfected either into suspension-adapted ExpiCHO cells (Thermo Fisher) or Expi293F (Thermo Fisher) cells with PEI MAX (Polysciences) in ProCHO5 medium (Lonza). After transfection, incubation with agitation was performed at 31°C and 4.5% CO2 for 5 days. The clarified supernatant was purified in two steps; via a Strep-Tactin XT column (IBA Lifesciences) followed by Superose 6 10/300 GL column (GE Healthcare) and finally dialyzed into PBS. The average yield was 15 mg/L culture.

Yale, New Haven. Human codon optimized SARS-CoV (2003) RBD (pEZT containing H7 leader sequence; aa. 306-527, C-terminal Avi- and 8His tags) was transiently transfected into Expi293™ cells (Thermo Fisher) using the ExpiFectamine™ 293 Transfection kit (Gibco) according to the manufacturer's instructions. Cells were cultured in a 37˚C incubator with 8% humidified CO_2 for 4 days after transfection. Culture supernatant was collected by centrifugation (500 x g for 10 minutes) and RBD was captured using Ni-NTA Superflow resin (Qiagen), washed, and eluted in buffer containing 50 mM Tris-HCl pH 8, 350 mM NaCl, and 250 mM imidazole. RBD was further purified using an ENrich™ SEC 650 column (Bio-Rad) equilibrated in 1X PBS (Thermo Fisher). Peak fractions were pooled and the protein concentration was determined by 280 nm absorbance with a Nanodrop™ One Spectrophotometer (Thermo Fisher). Protein was snap frozen in liquid nitrogen and shipped on dry ice prior to experiments.

Zurich, ETH. NSP1 carrying an N-terminal His6-tag followed by a TEV cleavage site was expressed from a pET24a vector. The plasmid was transformed into E. coli BL21-CodonPlus (DE3)-RIPL and cells were grown in 2xYT medium at 30 °C. At an OD600 of 0.8, cultures were shifted to 18 °C and induced with IPTG to a final concentration of 0.5 mM. After 16 h, cells were harvested by centrifugation, resuspended in lysis buffer (50 mM HEPES-KOH pH 7.6, 500 mM KCl, 5 mM MgCl2, 40 mM imidazole, 10% (w/v) glycerol, 0.5 mM TCEP and protease inhibitors) and lysed using a cell disrupter (Constant Systems Ltd). The lysate was cleared by centrifugation for 45 min at 48.000 xg and loaded onto a HisTrap FF 5-ml column (GE Healthcare). Eluted proteins were incubated with TEV protease at 4 °C overnight and the His6-tag, uncleaved NSP1 and the His6-tagged TEV protease were removed on the HisTrap FF 5-ml column. The sample was further purified via size-exclusion chromatography on a HiLoad 16/60 Superdex75 (GE Healthcare),

buffer exchanging the sample to the storage buffer (40 mM HEPES-KOH pH 7.6, 200 mM KCl, 40 mM MgCl2, 10% (w/v) glycerol, 1 mM TCEP). Fractions containing NSP1 were pooled, concentrated in an Amicon Ultra-15 centrifugal filter (10-kDa MW cut-off), flash-frozen in liquid nitrogen, and stored until further use at -80 °C.

Details of viral proteins used for this study

For *high-throughput serology*, the following proteins were used: SARS-CoV-2 S (pHL-Sec; aa. 1-1208, C-terminal 8His-Twin-Strep) and RBD (pOPINTTGNeo; aa. 330-532, C-terminal 6His) produced at the SGC in Oxford and the nucleocapsid protein from AcroBiosystems (AA Met 1 - Ala 419, C-terminal his-tag, NUN-C5227). For *competitive ELISA*, we used: The prefusion ectodomain of the SARS-CoV-2 S protein (Lausanne, EPFL SV PTECH PTPSP), the RBD from Trenzyme (C-terminal his-tag, P2020-001) and the nucleocapsid protein from AcroBiosystems (AA Met 1 - Ala 419, C-terminal his-tag, NUN-C5227). For *additional ELISAs* following the high-throughput serology, we used: The prefusion ectodomain of the SARS-CoV-2 S protein (Lausanne, EPFL SV PTECH PTPSP), the RBD from Trenzyme (C-terminal his-tag, P2020-001) and, nucleocapsid protein from AcroBiosystems (AA Met 1 - Ala 419, C-terminal his-tag, NUN-C5227), the SARS-COV-2 NSP1 protein (from Nenad Ban, ETH Zurich), the CMV pp65 protein (Abcam, ab43041), and BSA (Thermo Scientific).

Western Blotting

Expi293F cells were obtained as a gift from Prof. Maurizio Scaltriti (Memorial Sloan Kettering Cancer Center, New York). Non transfected control cells and cells overexpressing either His-tagged S, His-tagged NC or His-tagged RBD domain were lysed in 0,1% Triton X-100/PBS. Total protein content in the cellular fraction was quantified using bicinchoninic protein assay (Pierce BCA Protein Assay Kit, ThermoFisher). For Western Blotting, 30 µg of ECD-expressing lysate, 10 µg of NC-expressing lysate and 10 µg of RBD-expressing lysate were loaded all in the same well of NU-PAGE 4-12% Bis-Tris gels (ThermoFisher). 50 µg of non-transfected cell lysate were loaded as negative control. Gels were run at a constant voltage (150 V) in MES running buffer for 50 minutes, then transferred onto PVDF membrane with a dry transfer system (iBlot 2 Gel Transfer Device, ThermoFisher). The membranes were blocked with 5% SureBlock (Lubio Science) for 1 hour at room temperature, and then incubated overnight with a 1:100 dilution of patients' plasma in 1% SureBlock, at 4 degrees. The day after, membranes were washed four times with PBS-T and incubated for 1 hours with an anti-human secondary antibody, HRP-conjugated, diluted 1:10000 in 1% SureBlock. The membranes were then washed four times with PBS-T and acquired

using Immobilon Crescendo HRP Substrate (Merck Millipore) and Fusion SOLO S imaging system (Vilber). As a positive control, one membrane was incubated overnight with mouse anti-Histag antibody (ThermoFisher, dilution 1:10000 in 1% SureBlock) and subsequently with anti-mouse secondary antibody, HRP-conjugated (Jackson, dilution 1:10000 in 1% SureBlock).

Competitive ELISA

To perform competitive ELISAs, high-binding 384-well plates (Perkin Elmer, SpectraPlate 384 HB) were coated with 1 ug/mL S or RBD or NC in PBS at 37°C for 1 h, followed by 3 washes with PBS-T and by blocking with 5% milk in PBS-T for 1.5 h. Meanwhile, plasma samples were diluted to a final concentration close to the EC_{50}, incubated with either RBD (50 ug/mL) or S (12.5 ug/mL) and serially diluted (11 dilution points per patient sample, 25 uL per dilution) in a low-binding 384-well plates (Perkin Elmer, high binding SpectraPlate). After 2 h of incubation at RT, 20 uL of all the samples were transferred to the previously coated plates and incubated for additional 2 h at RT. Then, the plates were washed five times with PBS-T and the presence of IgGs was detected using an HRP-linked anti-human IgG antibody (Peroxidase AffiniPure Goat Anti-Human IgG, Fcγ Fragment Specific, Jackson, 109-035-098, at 1:4000 dilution in sample buffer). The incubation of the secondary antibody for one hour at RT was followed by three washes with PBS-T, the addition of TMB, an incubation of 5 minutes at RT, and the addition of 0.5 M H2SO4. The absorbance at 450 nm was measured in a plate reader (Perkin Elmer, EnVision) and the inflection points of the sigmoidal binding curves were determined using a custom designed fitting algorithm.

Microscale diffusional sizing

For the microfluidic binding measurements, 40% of human plasma was added to 10 nM antigen and PBS was added to give a constant volume of 20 µL. The antigen used was RBD labelled with Alexa Fluor 647 through N-terminal amine coupling. These samples were incubated at room temperature for 40 minutes and the size, hence molecular weight of the formed immunocomplex, was determined through measuring the hydrodynamic radius, Rh with microfluidic diffusional sizing (32) using a Fluidity One W platform (Fluidic Analytics, Cambridge, UK). Following correction of fluorescence intensities for serum autofluorescence, the fraction, f_d, of RBD to diffuse into the distal channel is defined by:

$$f_d = \frac{[AbR](1-\rho_b) + ([R]_0 - [AbR](1-\rho_f))}{[R]_0}$$

Where [*AbR*] is the concentration of bound RBD, $[R]_0$ is the total concentration of RBD, and ρ_b and ρ_f are the fractions of bound and free RBD to diffuse into the distal channel, respectively.

References

1. Bendavid E, Mulaney B, Sood N, Shah S, Ling E, Bromley-Dulfano R, et al. COVID-19 Antibody Seroprevalence in Santa Clara County, California. 2020:2020.04.14.20062463.
2. Kucirka LM, Lauer SA, Laeyendecker O, Boon D, Lessler J. Variation in False-Negative Rate of Reverse Transcriptase Polymerase Chain Reaction-Based SARS-CoV-2 Tests by Time Since Exposure. Ann Intern Med. 2020.
3. He X, Lau EHY, Wu P, Deng X, Wang J, Hao X, et al. Temporal dynamics in viral shedding and transmissibility of COVID-19. Nat Med. 2020;26(5):672-5.
4. Amanat F, Stadlbauer D, Strohmeier S, Nguyen THO, Chromikova V, McMahon M, et al. A serological assay to detect SARS-CoV-2 seroconversion in humans. Nat Med. 2020.
5. Okba NMA, Muller MA, Li W, Wang C, GeurtsvanKessel CH, Corman VM, et al. Severe Acute Respiratory Syndrome Coronavirus 2-Specific Antibody Responses in Coronavirus Disease 2019 Patients. Emerg Infect Dis. 2020;26(7).
6. Stadlbauer D, Amanat F, Chromikova V, Jiang K, Strohmeier S, Arunkumar GA, et al. SARS-CoV-2 Seroconversion in Humans: A Detailed Protocol for a Serological Assay, Antigen Production, and Test Setup. Curr Protoc Microbiol. 2020;57(1):e100.
7. Krystufek R, Sacha P. Increasing the throughput of crystallization condition screens: Challenges and pitfalls of acoustic dispensing systems. MethodsX. 2019;6:2230-6.
8. Kulesskiy E, Saarela J, Turunen L, Wennerberg K. Precision Cancer Medicine in the Acoustic Dispensing Era: Ex Vivo Primary Cell Drug Sensitivity Testing. J Lab Autom. 2016;21(1):27-36.
9. Song W, Gui M, Wang X, Xiang Y. Cryo-EM structure of the SARS coronavirus spike glycoprotein in complex with its host cell receptor ACE2. PLoS Pathog. 2018;14(8):e1007236.
10. Lemaitre JC, Perez-Saez J, Azman AS, Rinaldo A, Fellay J. Assessing the impact of non-pharmaceutical interventions on SARS-CoV-2 transmission in Switzerland. Swiss Med Wkly. 2020;150:w20295.
11. Tai W, Zhang X, He Y, Jiang S, Du L. Identification of SARS-CoV RBD-targeting monoclonal antibodies with cross-reactive or neutralizing activity against SARS-CoV-2. Antiviral Res. 2020;179:104820.
12. Streeck H, Schulte B, Kuemmerer B, Richter E, Hoeller T, Fuhrmann C, et al. Infection fatality rate of SARS-CoV-2 infection in a German community with a super-spreading event. 2020:2020.05.04.20090076.
13. Stringhini S, Wisniak A, Piumatti G, Azman AS, Lauer SA, Baysson H, et al. Seroprevalence of anti-SARS-CoV-2 IgG antibodies in Geneva, Switzerland (SEROCoV-POP): a population-based study. Lancet. 2020.
14. Pollan M, Perez-Gomez B, Pastor-Barriuso R, Oteo J, Hernan MA, Perez-Olmeda M, et al. Prevalence of SARS-CoV-2 in Spain (ENE-COVID): a nationwide, population-based seroepidemiological study. Lancet. 2020.
15. Sandri MT, Azzolini E, Torri V, Carloni S, Tedeschi M, Castoldi M, et al. IgG serology in health care and administrative staff populations from 7 hospital representative of different exposures to SARS-CoV-2 in Lombardy, Italy. 2020:2020.05.24.20111245.
16. BAG. Coronavirus Krankheit 2019 (COVID-19): Situationsbericht zur epidemiologischen Lage in der Schweiz und im Fürstentum Liechtenstein. (Version 28.05.2020). 2020.
17. Perez-Saez J, Lauer SA, Kaiser L, Regard S, Delaporte E, Guessous I, et al. Serology-informed estimates of SARS-CoV-2 infection fatality risk in Geneva, Switzerland. Lancet Infect Dis. 2020.
18. Hauser A, Counotte MJ, Margossian CC, Konstantinoudis G, Low N, Althaus CL, et al. Estimation of SARS-CoV-2 mortality during the early stages of an epidemic: A modeling study in Hubei, China, and six regions in Europe. PLoS Med. 2020;17(7):e1003189.

19. Seow J, Graham C, Merrick B, Acors S, Steel KJA, Hemmings O, et al. Longitudinal evaluation and decline of antibody responses in SARS-CoV-2 infection. 2020:2020.07.09.20148429.
20. Edridge AW, Kaczorowska JM, Hoste AC, Bakker M, Klein M, Jebbink MF, et al. Coronavirus protective immunity is short-lasting. 2020:2020.05.11.20086439.
21. Liu A, Li Y, Peng J, Huang Y, Xu D. Antibody responses against SARS-CoV-2 in COVID-19 patients. J Med Virol. 2020.
22. Ng K, Faulkner N, Cornish G, Rosa A, Earl C, Wrobel A, et al. Pre-existing and de novo humoral immunity to SARS-CoV-2 in humans. 2020:2020.05.14.095414.
23. Long QX, Tang XJ, Shi QL, Li Q, Deng HJ, Yuan J, et al. Clinical and immunological assessment of asymptomatic SARS-CoV-2 infections. Nat Med. 2020.
24. Robbiani DF, Gaebler C, Muecksch F, Lorenzi JCC, Wang Z, Cho A, et al. Convergent antibody responses to SARS-CoV-2 in convalescent individuals. Nature. 2020.
25. Le Bert N, Tan AT, Kunasegaran K, Tham CYL, Hafezi M, Chia A, et al. SARS-CoV-2-specific T cell immunity in cases of COVID-19 and SARS, and uninfected controls. Nature. 2020.
26. Altmann DM, Boyton RJ. SARS-CoV-2 T cell immunity: Specificity, function, durability, and role in protection. Sci Immunol. 2020;5(49).
27. Kirschenbaum D, Imbach LL, Ulrich S, Rushing EJ, Keller E, Reimann RR, et al. Inflammatory olfactory neuropathy in two patients with COVID-19. Lancet. 2020;396(10245):166.
28. Althaus CL, Probst D, Hauser A, Riou J. Time is of the essence: containment of the SARS-CoV-2 epidemic in Switzerland from February to May 2020. medRxiv. 2020.
29. openZH github repository: Statistisches Amt Kanton Zuerich; 2020 [Available from: https://github.com/openZH/covid_19.
30. Wrapp D, Wang N, Corbett KS, Goldsmith JA, Hsieh CL, Abiona O, et al. Cryo-EM structure of the 2019-nCoV spike in the prefusion conformation. Science. 2020;367(6483):1260-3.
31. Aricescu AR, Lu W, Jones EY. A time- and cost-efficient system for high-level protein production in mammalian cells. Acta Crystallogr D Biol Crystallogr. 2006;62(Pt 10):1243-50.
32. Arosio P, Muller T, Rajah L, Yates EV, Aprile FA, Zhang Y, et al. Microfluidic Diffusion Analysis of the Sizes and Interactions of Proteins under Native Solution Conditions. ACS Nano. 2016;10(1):333-41.

Acknowledgments

All authors wish to thank their entire teams for support in the lab. Linda Irpinio, André Wethmar, and Andra Chincisan are acknowledged for help in the lab and with data processing. Vishalini Emmenegger (ETH Zurich) offered insightful advice and kind help with illustrations. We are grateful to Elisabeth J. Rushing (USZ) for proofreading the manuscript, to Guido Bucklar, Michael Fetzer, Katie Kalt, Karin Edler, Roland Naef, and especially Patrick Hirschi (USZ) for their help with hospital data, and to Didier Trono for helpful insights and discussions. Michael Weisskopf, Regina Grossmann and the team of the Clinical Trials Center (CTC) of the USZ are acknowledged for their help with sample acquisition and protocols. Above all, we are grateful to all blood donors and hospital patients for helping us conduct this study.

Funding

Institutional core funding by the University of Zurich and the University Hospital of Zurich to AA, as well as Driver Grant 2017DRI17 of the Swiss Personalized Health Network to AA. The robotic rig was acquired with an R'Equip grant of the Swiss National Foundation to AA. Screening methodologies had been developed thank to the support of an Advanced Grant of the European Research Council and a Distinguished Scientist Award of the Nomis Foundation to AA. Funding by grants of Innovation Fund of the University Hospital Zurich to AA, AvE, DS, EPM, ME, and OB. Access to the Creoptix WAVE system was kindly provided by Creoptix AG. Wädenswil, CH. Utilization of the Fluidity One-W was kindly granted by Fluidic Analytics, Cambridge, UK. This work was supported by ETH Research Grant ETH-23 18-2 and a Ph.D. fellowship by Boehringer Ingelheim Fonds to KS. Raphaël Jacquat acknowledges funding by the EPSRC for Doctoral Training in Sensor Technologies and Applications (grant EP/L015889/1). ICM acknowledges funding by the Swiss Government FCS. Carlo Cervia was funded by a Swiss Academy of Medical Sciences fellowship (#323530-191220). GFXS was supported by an COVID-19 Emergency Fund of the Director of PSI. TM is supported by Cancer Research UK grants C20724/A14414 and C20724/A26752 to Christian Siebold (Oxford). Oxford work was supported by the MRC and Chinese Academy of Medical Sciences Innovation Fund for Medical Science, China Grant 2018-I2M-2-002. GRS is supported as a Wellcome Trust Senior Investigator (grant 095541/A/11/Z) and receives funding from the National Institute for Health Research Biomedical Research Centre Funding Scheme. CA received funding from the European Union's Horizon 2020 research and innovation programme - project EpiPose (No 101003688) and the Swiss National Science Foundation (grant 196046).

Author contributions

Collected and processed the biological specimens, prepared and carried out the high-throughput screenings, maintained the machines: ME, DS, BD, JG, AW, MI, JD, CZ. Analyzed data from the high-throughput serology: DL, RJ, IX, ME, AA. Carried out follow-up ELISAs and competitive ELISAs: EDC, RM, ME. Carried out Western Blots: EDC, CT, AGG. Carried out and interpreted experiments in solution using microfluidics diffusional sizing technology: MMS, ICM, CKX, GM, TJPK, VK, ME, AA. Collected samples from COVID-19 patients for the establishment of serology: ILD, DJS. Coordinated the sample acquisition and processing from the Institute of Clinical Chemistry: AvE and LS. Coordinated the sample acquisition and processing from the blood donation services: BF and JG. Coordinated and performed high-throughput ELISAs for comparison in Oxford: DE, StH, DIS. Coordinated and performed SARS-CoV-2 serological assays using commercial platforms: LS, KS, AvE, EPM, OB. Produced proteins: DIS, NBB, RO, TM, FP, DH, KL, EDC, JDH, FL, AMR, SH, GS. Carried out the epidemiological modeling: CA. Coordinated the correspondence with the ethics committee of the Kanton of Zurich: RR, JN, ME. Produced and redacted the figures: AA, RJ, DL, EDC, ME. Conceived the idea of creating a biobank of plasma samples, supervised the study on a daily basis, proposed primary and confirmatory experiments, advised on best lab practices, on control experiments and on data interpretation: AA. Wrote abstract, introduction and discussion: AA. Wrote a first draft of the Results part of the manuscript: ME. Advised on and corrected the Results section: AA. All authors contributed by reviewing the first draft, approved the final version, and consented to be accountable for the work.

Competing interests

TPJK is a member of the board of directors of Fluidic Analytics. AA is a member of the board of directors of Mabylon AG which has funded antibody-related work in the Aguzzi lab in the past. All other authors declare no competing interests.

Data and materials availability

The raw data underlying this study will be made available upon reasonable request. The biobank samples are limited and were exhausted in several instances. Therefore, while we will make efforts to provide microliter amounts of samples to other researchers, their availability is physically limited.

Figure Legends:

Fig. 1. Study overview and establishment of serological pipeline. A. To estimate the prevalence of SARS-CoV-2 seropositivity in the population, prepandemic and copandemic samples from two independent cohorts were analyzed by high-throughput microELISA (TRABI). IgG titers against S, RBD and NC were determined and the –log(EC_{50}) was inferred by regression analysis. **B**. Vero cells infected with SARS-CoV-2 (lane 2), but not uninfected cells (lane 1), showed signals corresponding to S (black arrow) and NC (blue arrow, pointing at two bands) when immunoblotted with COVID-19 patient plasma. NC protein undergoes a proteolytic cleavage in SARS-CoV infected VeroE6 cells, resulting in two distinct bands of around 46 and 43 kDa. We confirmed the identity of the two bands by probing with an anti-NC antibody (Sino Biologicals, data not shown). Spiking of COVID-19 patient plasma with recombinant S and NC led to the disappearance of all signals. **C**. Upper panel: Using 53 samples from confirmed SARS-CoV-2 patients and 83 prepandemic samples, we assessed the specificity-sensitivity relationship for all antigens individually and after combining all results into a single score (TRABI) using QDA-based posterior probability. Between 7 and 13 dpo, approximately 60% of samples were positive (posterior probability >0.5) at 100% specificity cutoff, whereas 100% sensitivity was reached at ≥ 14 dpo. Lower panel: COVID and prepandemic samples were used to assess the performance of TRABI, commercial tests (Roche, DiaSorin, Abbott, Euroimmun) and an assay developed at the Target Discovery Institute (Oxford). While all tests scored equally at ≥14 dpo, TRABI outperformed all other assays at ≤13 dpo. **D**. Time course of IgG response in 55 samples from 27 COVID patients. IgG antibodies were reliably detectable at ≥13 dpo. Colors represent individual patients.

Fig. 2. Evolution of SARS-CoV-2 prevalence in a cohort of Zurich University Hospital (USZ) patients and donors from the blood donation service (BDS). **A-B**. Inflection points of dilution curves, denoted -log(EC_{50}), of plasma titrated against S and RBD in the USZ and BDS cohorts. Posterior probabilities were calculated using QDA assuming a multivariate Gaussian distribution. **C**. Prevalence of SARS-CoV-2 seropositivity in prepandemic (before December 2019) and copandemic samples (from December 2019 to July 2020) estimated using the posterior probabilities from the multivariate Gaussian distribution. Bar: 95% confidence intervals (CI). **D**. Modelled seroprevalence fitted to data from BDS. **E**. TRABI reproducibility was assessed using duplicates run in pairs of independent assay plates. **F**. To assess potential cross-reactivity of SARS-CoV-2 seropositive individuals, we tested 210 high-scoring samples and 122 random samples for binding

to the RBD of SARS-CoV. SARS-CoV-2 RBD binders with a high posterior probability (same color maps as in B) segregated within the higher anti-SARS-CoV-RBD titers.

Fig. 3. Demographic and clinical annotations of the tested cohorts. **A**. and **B**. Age and gender pyramids for the USZ (A) and the BDS (B) cohorts with indications of the respective posterior probability ($p > 0.5$). A contour of the respective age pyramid for the inhabitants of the Canton of Zurich was drawn based on data provided by the statistical service of the Canton of Zurich. The narrower age spectrum of blood donors reflects regulatory restrictions of donation. **C**. Total samples (dark blue) and seropositive samples (light blue) stratified by the geographic residence of sample donors. **D**. Distribution of plasma samples by clinical departments of the hospital (dark blue: totals; light blue: posterior probability > 0.5). **E**. Individual time courses for repeat samples of patients annotated to be SARS-CoV-2 PCR-positive. Shown is the reactivity against the S protein, for time frames of up to 100 days. Colors represent individual patients.

Fig. 4. Characterization of prepandemic samples. **A**. Posterior probability were calculated assuming a Gaussian distribution and visualized for individual antigens (S, RBD and NC) for prepandemic samples vs. copandemic USZ samples drawn in May and June 2020. Prepandemic samples exhibited a low posterior probability as they typically reacted against single antigens, leading to low rankings in a composite metric. For further testing, comparative samples were chosen from the prepandemic era and from May and June 2020. Arrows point to samples of individuals used in (B), (C), (D). P1-6: prepandemic 1-6; C1-2: COVID1-2. **B**. Western Blot analysis of two samples from May/June 2020 (“COVID 1” and “COVID 2”) and several prepandemic samples (denoted with 2, 4 and 5). Anti-his-tag antibody was included as a positive control. Lane 1 = non-transfected Expi293F cell lysate; Lane 2 = Expi293F cell lysates expressing his-tagged S, NC and RBD proteins. Black arrows: S; blue arrows: NC; purple arrow: RBD. **C.** ELISA assays on the same samples as in B, using SARS-CoV-2 S, NC, RBD and NSP1 as well as control proteins (BSA, CMV pp65). **D**. Soluble recombinant S or RBD were spiked into plasma at 0.04-88 nM (S) and 0.7-1350 nM (RBD), in the same samples as in B and C, and ELISA was then performed with immobilized RBD or S. Data points represent averages of duplicates. Soluble antigens suppressed the ELISA signal in the COVID samples but not in the prepandemic sample, showing that the antibodies present in the latter had lower affinities for SARS-CoV-2 targets.

Fig. 5. Assay validation in solution and clonality of anti-S immune response. **A**. ELISA assays of healthy blood donors vs. convalescent individuals. **B**. Microfluidic-based assessment of binding between an Alexa 647-labelled RBD antigen and antibodies in solution. No change in diffusion coefficient or the associated hydrodynamic radius was observed in control samples, while all ELISA-positive samples from convalescent and healthy donors indicated a clear binding of antibodies to RBD, confirming the ELISA-based results. **C**. Western Blot analysis of the same individuals tested in (A). Lane 1 = non-transfected Expi293F cell lysate; Lane 2 = Expi293F cell lysates expressing his-tagged S, NC and RBD proteins. Black arrows: S. Blue arrows: NC. **D**. Competitive ELISA using RBD or S for soluble competition with antibodies in plasma from the same individuals as in (A) and (C). Each point is the average of duplicates with error bars except for “donor 4” in the competitive ELISA using soluble RBD and immobilization for RBD which is a unicate.

Supplementary Materials:

Fig. S1. **Detailed assay procedure**. **A**. Sample acquisition. **B**. Experimental workflow using high-throughput screening platform.

Fig. S2. Comparison of TRABI to a lateral-flow assay developed by Bloom diagnostics.

Fig. S3. **Prevalence estimation in two large cohorts**. **A**. and **B**. Half-violin plots showing the distribution of anti-S/RBD/NC reactivity in the –log(EC_{50}) scale for the USZ (A) and the BDS (B) cohort. Color bar: posterior probability **C.** and **D**. Depicted are all the –log(EC_{50}) values calculated for S and the RBD for the USZ (C) and the BDS (D) cohort. Posterior probability were calculated using LDA. **E**. and. **F**. Q-Q plots to check the Gaussian distributional assumption of the LDA model. For USZ (E) and the BDS (F) cohort respectively, we collapsed the 3 measures per sample according to the linear discriminant classifier. We then scaled known positives and negatives to mean zero and unit variance and compared their distributions to the univariate Gaussian distribution via Q-Q plot. We saw that for the relevant upper tail, the distribution of known negatives followed the normal distribution with only a mild deviation, such that, for instance, the upper one percent quantile is reached at 2.04 (E) and 2.00 (F) rather than at their theoretical value of 2.32. **G**. and. **H**. ROC curves for the USZ (G) and BDS (H) cohorts using the prepandemic samples (including the ones from December 2019 and January 2020 for BDS) as condition negatives and selected condition positives from both cohorts. **I**. Using the posterior probabilities from the LDA, the prevalence of SARS-CoV-2 seropositivity was calculated in prepandemic samples and then from December 2019 to July 2020.

Fig. S4. Epidemiological modelling. Modelled number of hospitalized (A) and ventilated (B) patients and deaths (C) during the SARS-CoV-2 epidemic in the Canton of Zurich, Switzerland. The solid lines show the maximum likelihood estimate of the model and the shaded areas correspond to the 95% prediction intervals. The model was fitted to the data indicated as white circles and the BDS seroprevalence estimates as shown in Fig. 2D.

Fig. S5. Assay reproducibility using 210 high scoring samples and 122 random samples (based on results from the high-throughput screen) for binding against S, the RBD, and

the NC. **A.** S binding shows that reproducibility increases at higher values, consistent with increased posterior probabilities. **B.** Same observation as (A) for the RBD. **C**. Same observation as (A) for the NC.

Fig. S6. Characterization of prepandemic and copandemic samples. **A**. Western Blot analysis. For a better visualization, brightness and contrast have been modified and the images have been partially cropped. Original images are shown in Fig. S6. **B**. Additional ELISA. **C**. Competitive ELISA.

Fig. S7. Competitive ELISA probing for NC signal for healthy blood donors and convalescent individuals.

Fig. S8. Uncropped and unmodified camera-acquired images of the Western Blots displayed in Figs. 4 and 5 and Fig. S6.

Table S1. Descriptive statistics of age and sex for all cohorts. Data shown here show basic annotations for the USZ as well as for the BDS cohort. Samples from the BDS cohort were fully anonymized until March. Demographic and clinical annotations are only available since April 2020 for bioethical reasons.

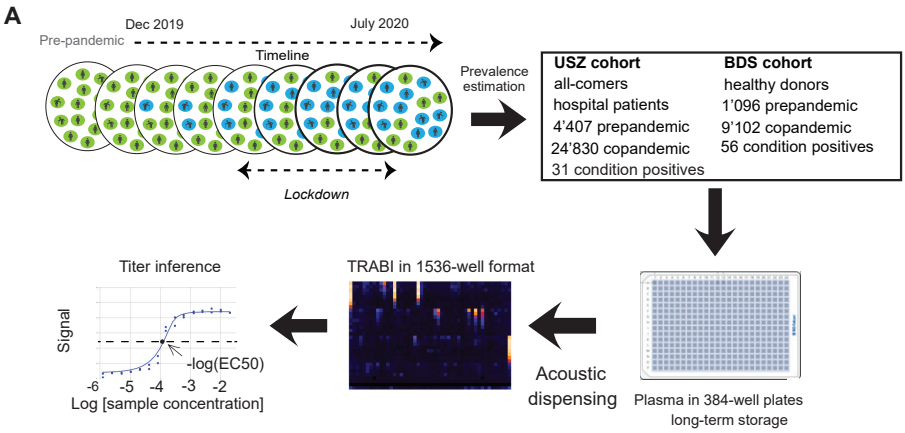
A
Dec 2019
July 2020
Pre-pandemic
Timeline
Lockdown
Prevalence estimation
USZ cohort
all-comers
hospital patients
4'407 prepandemic
24'830 copandemic
31 condition positives
BDS cohort
healthy donors
1'096 prepandemic
9'102 copandemic
56 condition positives
Plasma in 384-well plates
long-term storage
Acoustic dispensing
TRABI in 1536-well format
Titer inference
Signal
-log(EC50)
Log [sample concentration]

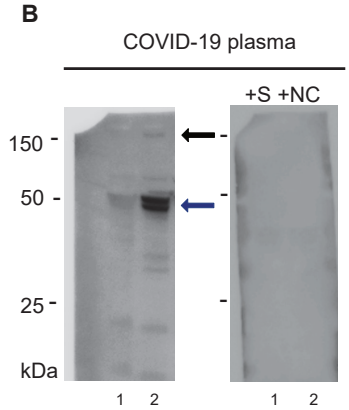
B
COVID-19 plasma
+S +NC
150
50
25
kDa
1
2
1
2

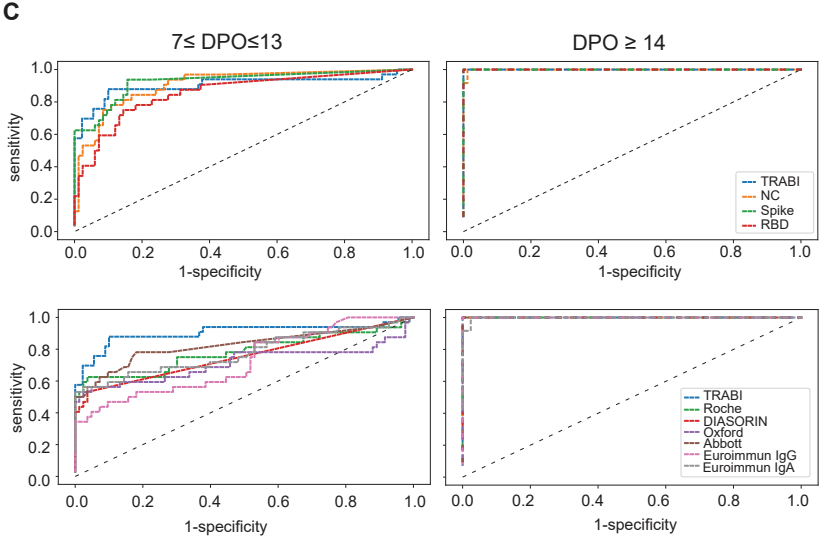
C
7≤ DPO≤13
DPO ≥ 14
sensitivity
1-specificity
TRABI
NC
Spike
RBD
TRABI
Roche
DIASORIN
Oxford
Abbott
Euroimmun IgG
Euroimmun IgA

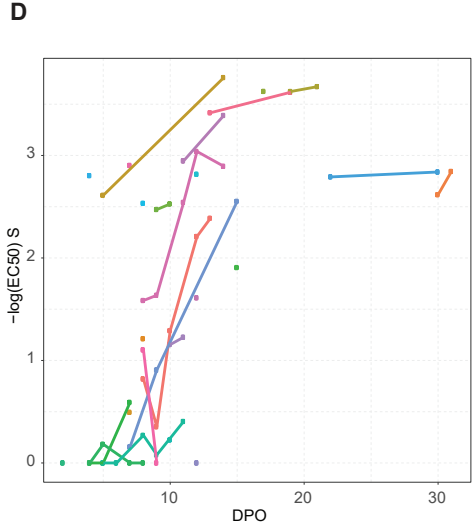
D
−log(EC50) S
DPO

Fig. 1

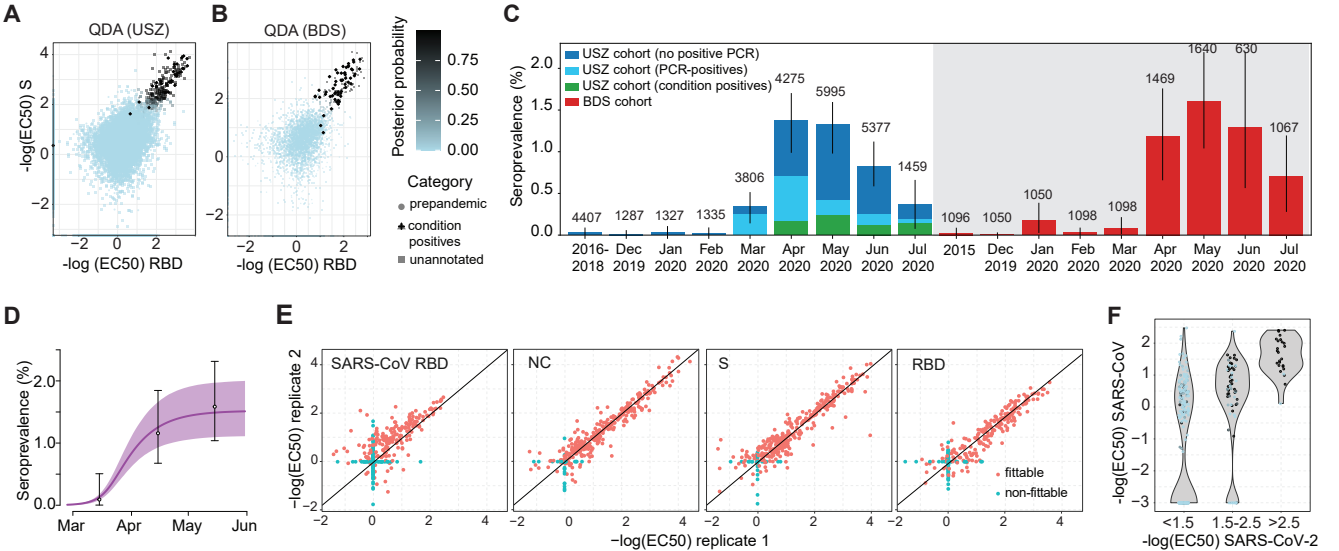
A
QDA (USZ)
-log(EC50) S
-log (EC50) RBD
B
QDA (BDS)
-log (EC50) RBD
Posterior probability
0.75
0.50
0.25
0.00
Category
prepandemic
condition positives
unannotated
C
USZ cohort (no positive PCR)
USZ cohort (PCR-positives)
USZ cohort (condition positives)
BDS cohort
Seroprevalence (%)
4407
1287
1327
1335
3806
4275
5995
5377
1459
1096
1050
1050
1098
1098
1469
1640
630
1067
2016-2018
Dec 2019
Jan 2020
Feb 2020
Mar 2020
Apr 2020
May 2020
Jun 2020
Jul 2020
2015
Dec 2019
Jan 2020
Feb 2020
Mar 2020
Apr 2020
May 2020
Jun 2020
Jul 2020
D
Seroprevalence (%)
Mar
Apr
May
Jun
E
SARS-CoV RBD
NC
S
RBD
−log(EC50) replicate 2
−log(EC50) replicate 1
fittable
non-fittable
F
-log(EC50) SARS-CoV
<1.5
1.5-2.5
>2.5
-log(EC50) SARS-CoV-2

Fig. 2

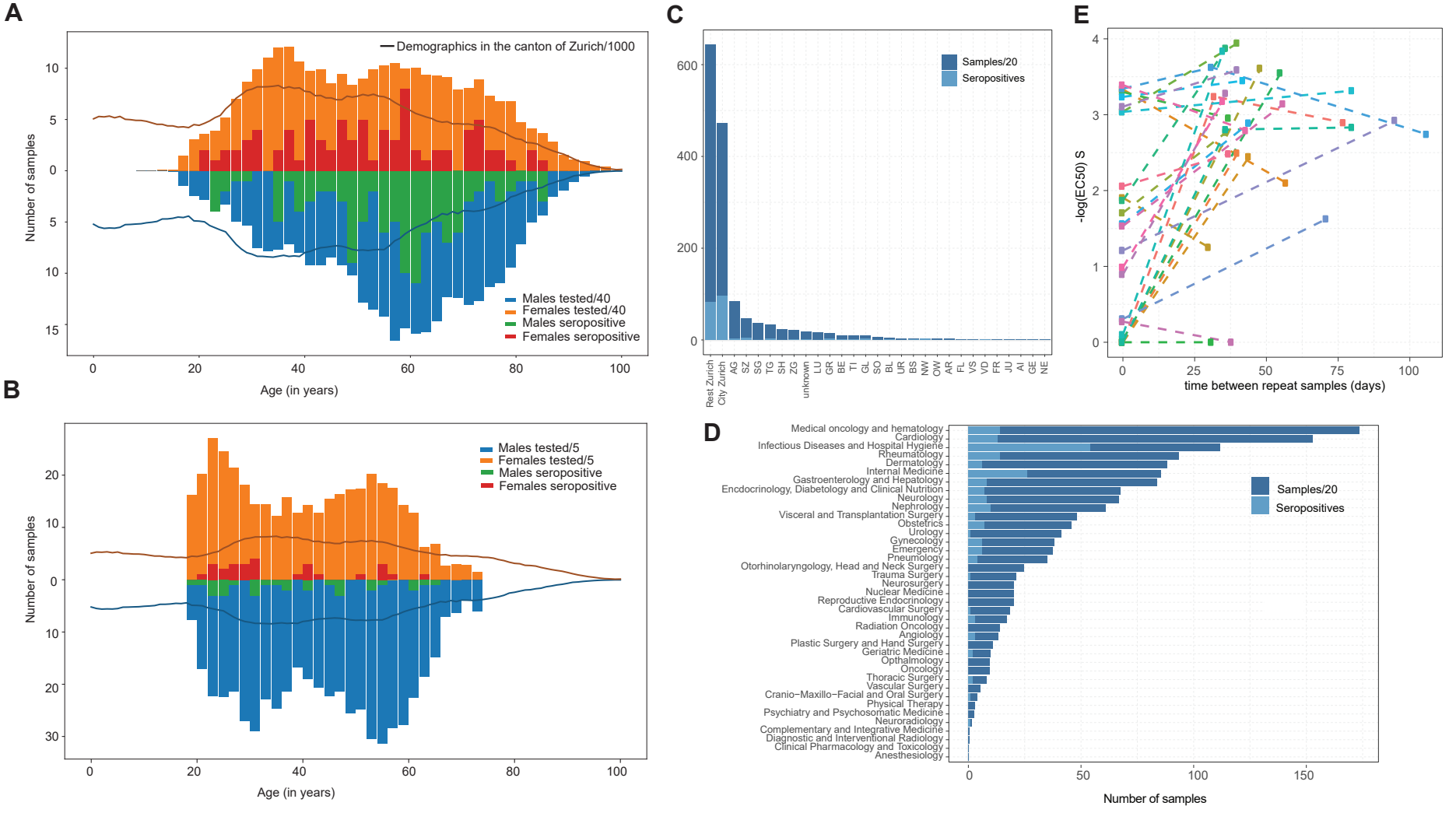
A
Demographics in the canton of Zurich/1000
Number of samples
Age (in years)
Males tested/40
Females tested/40
Males seropositive
Females seropositive
B
Males tested/5
Females tested/5
Males seropositive
Females seropositive
Number of samples
Age (in years)
C
Samples/20
Seropositives
Rest Zurich
City Zurich
AG SZ SG TG SH ZG unknown LU GR BE TI GL SO BL UR BS NW OW AR FL VS VD FR JU AI GE NE
E
-log(EC50) S
time between repeat samples (days)
D
Medical oncology and hematology
Cardiology
Infectious Diseases and Hospital Hygiene
Rheumatology
Dermatology
Internal Medicine
Gastroenterology and Hepatology
Encdocrinology, Diabetology and Clinical Nutrition
Neurology
Nephrology
Visceral and Transplantation Surgery
Obstetrics
Urology
Gynecology
Emergency
Pneumology
Otorhinolaryngology, Head and Neck Surgery
Trauma Surgery
Neurosurgery
Nuclear Medicine
Reproductive Endocrinology
Cardiovascular Surgery
Immunology
Radiation Oncology
Angiology
Plastic Surgery and Hand Surgery
Geriatric Medicine
Opthalmology
Oncology
Thoracic Surgery
Vascular Surgery
Cranio−Maxillo−Facial and Oral Surgery
Physical Therapy
Psychiatry and Psychosomatic Medicine
Neuroradiology
Complementary and Integrative Medicine
Diagnostic and Interventional Radiology
Clinical Pharmacology and Toxicology
Anesthesiology
Samples/20
Seropositives
Number of samples

Fig. 3

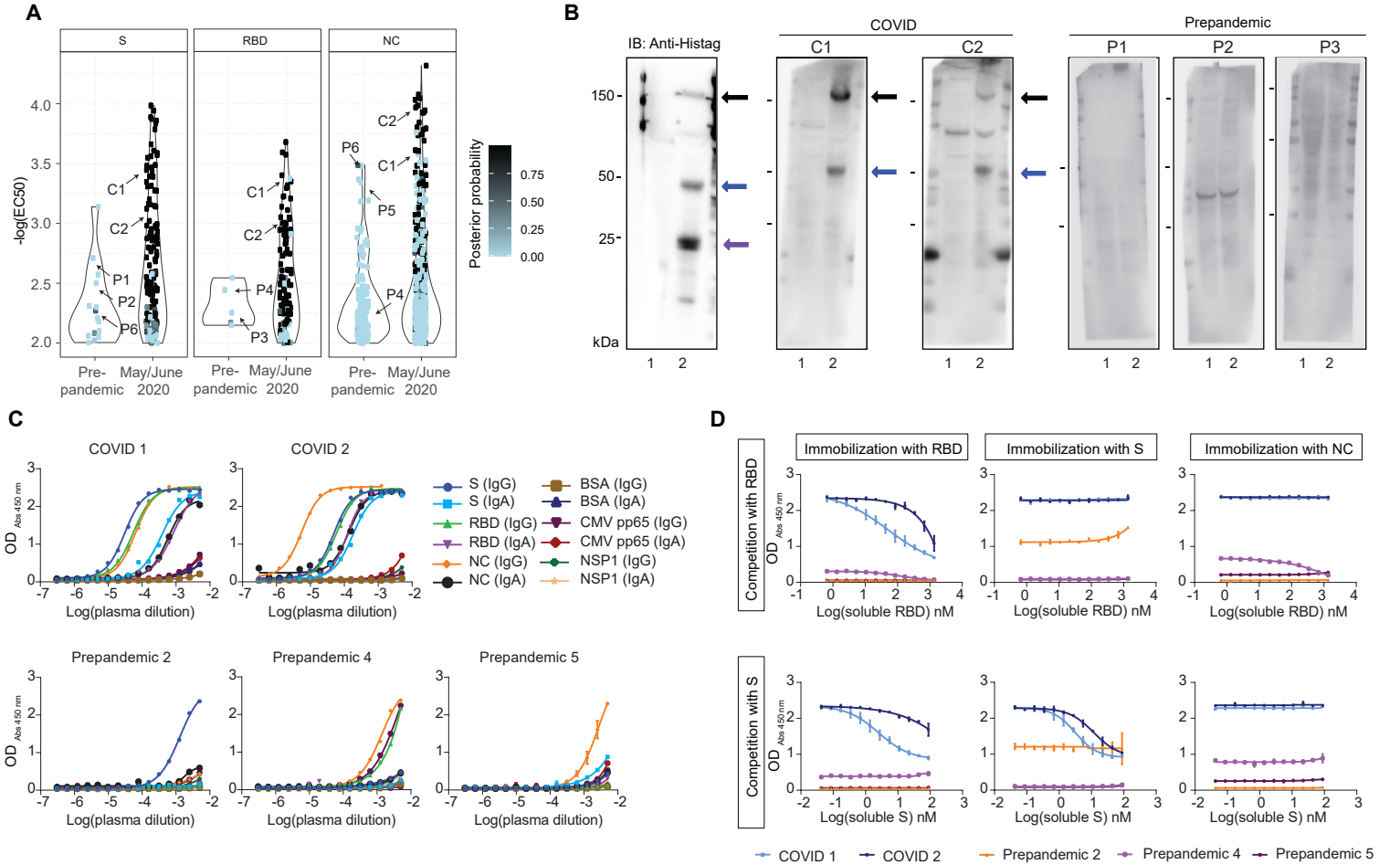
A
S
RBD
NC
-log(EC50)
4.0
3.5
3.0
2.5
2.0
C1
C2
P1
P2
P6
P3
P4
P5
Pre-pandemic
May/June 2020
Posterior probability
0.75
0.50
0.25
0.00
B
IB: Anti-Histag
COVID
Prepandemic
C1
C2
P1
P2
P3
150
50
25
kDa
1
2
C
COVID 1
COVID 2
Prepandemic 2
Prepandemic 4
Prepandemic 5
OD Abs 450 nm
Log(plasma dilution)
S (IgG)
S (IgA)
RBD (IgG)
RBD (IgA)
NC (IgG)
NC (IgA)
BSA (IgG)
BSA (IgA)
CMV pp65 (IgG)
CMV pp65 (IgA)
NSP1 (IgG)
NSP1 (IgA)
D
Immobilization with RBD
Immobilization with S
Immobilization with NC
Competition with RBD
Competition with S
Log(soluble RBD) nM
Log(soluble S) nM
COVID 1
COVID 2
Prepandemic 2
Prepandemic 4
Prepandemic 5

Fig. 4

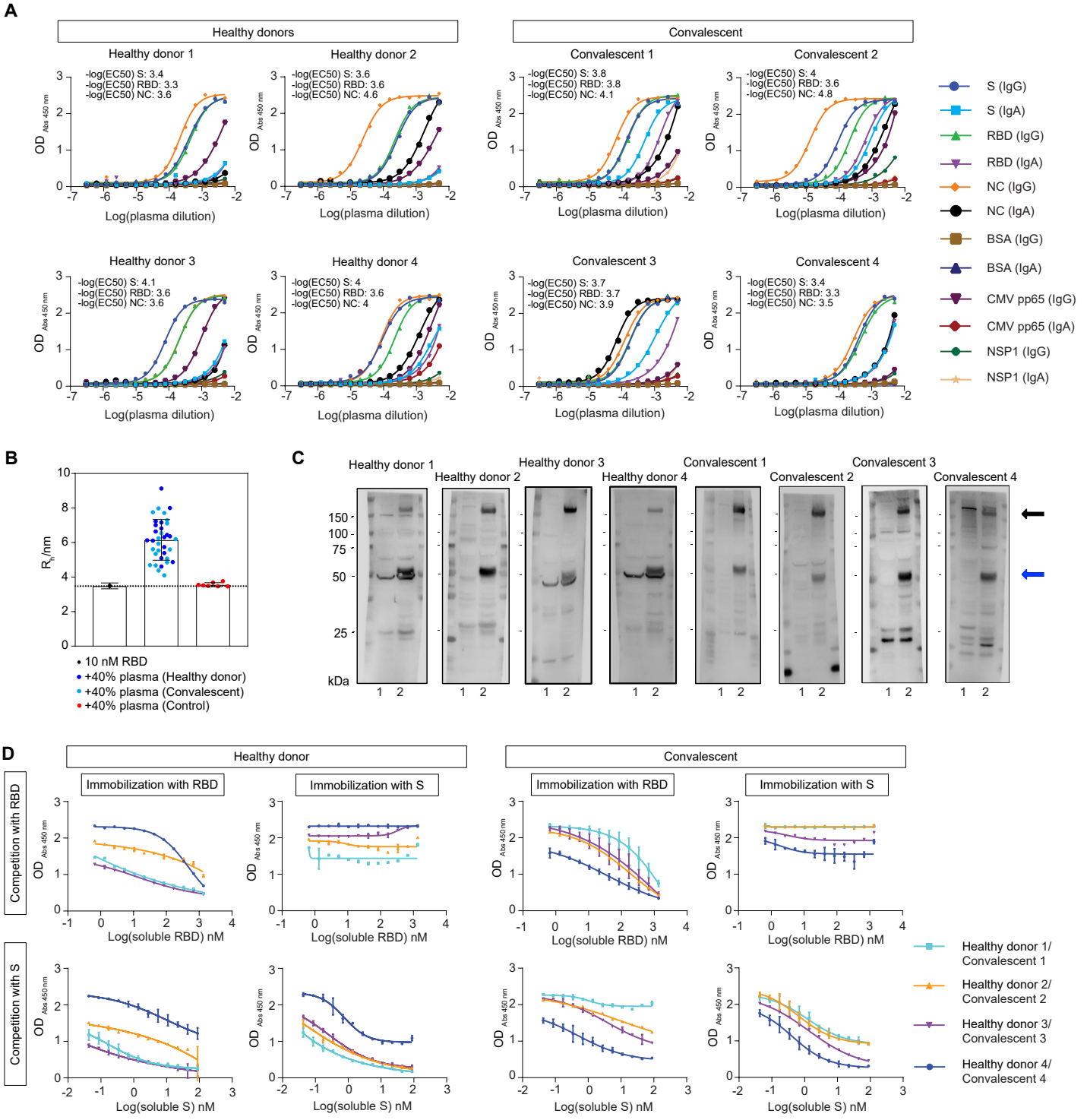
A
Healthy donors
Convalescent
Healthy donor 1
-log(EC50) S: 3.4
-log(EC50) RBD: 3.3
-log(EC50) NC: 3.6
Healthy donor 2
-log(EC50) S: 3.6
-log(EC50) RBD: 3.6
-log(EC50) NC: 4.6
Convalescent 1
-log(EC50) S: 3.8
-log(EC50) RBD: 3.8
-log(EC50) NC: 4.1
Convalescent 2
-log(EC50) S: 4
-log(EC50) RBD: 3.6
-log(EC50) NC: 4.8
Healthy donor 3
-log(EC50) S: 4.1
-log(EC50) RBD: 3.6
-log(EC50) NC: 3.6
Healthy donor 4
-log(EC50) S: 4
-log(EC50) RBD: 3.6
-log(EC50) NC: 4
Convalescent 3
-log(EC50) S: 3.7
-log(EC50) RBD: 3.7
-log(EC50) NC: 3.9
Convalescent 4
-log(EC50) S: 3.4
-log(EC50) RBD: 3.3
-log(EC50) NC: 3.5
OD Abs 450 nm
Log(plasma dilution)
S (IgG)
S (IgA)
RBD (IgG)
RBD (IgA)
NC (IgG)
NC (IgA)
BSA (IgG)
BSA (IgA)
CMV pp65 (IgG)
CMV pp65 (IgA)
NSP1 (IgG)
NSP1 (IgA)
B
R0/nm
10 nM RBD
+40% plasma (Healthy donor)
+40% plasma (Convalescent)
+40% plasma (Control)
C
Healthy donor 1
Healthy donor 2
Healthy donor 3
Healthy donor 4
Convalescent 1
Convalescent 2
Convalescent 3
Convalescent 4
150
100
75
50
25
kDa
1 2
D
Healthy donor
Convalescent
Immobilization with RBD
Immobilization with S
Competition with RBD
Competition with S
Log(soluble RBD) nM
Log(soluble S) nM
Healthy donor 1/ Convalescent 1
Healthy donor 2/ Convalescent 2
Healthy donor 3/ Convalescent 3
Healthy donor 4/ Convalescent 4

Fig. 5